Interplay between Coulomb-focusing and non-dipole effects in strong-field ionization with elliptical polarization

Author(s):
Daněk, Jiří; Klaiber, Michael; Hatsagortsyan, Karen Z.; Keitel, Christoph H.; Willenberg, Benjamin; Maurer, Jochen; Mayer, Benedikt W.; Phillips, Christopher R.; Gallmann, Lukas; Keller, Ursula

Publication date:
2018-05-14

Permanent link:
https://doi.org/10.3929/ethz-b-000268933

Originally published in:
Journal of Physics B: Atomic, Molecular and Optical Physics 51(11), https://doi.org/10.1088/1361-6455/aaba42

Funding acknowledgement:
320401 - Clocking fundamental attosecond electron dynamics (EC)

Interplay between Coulomb-focusing and non-dipole effects in strong-field ionization with elliptical polarization

OPEN ACCESS
IOP Publishing
Journal of Physics B: Atomic, Molecular and Optical Physics
J. Phys. B: At. Mol. Opt. Phys. **51** (2018) 114001 (16pp)
https://doi.org/10.1088/1361-6455/aaba42

Interplay between Coulomb-focusing and non-dipole effects in strong-field ionization with elliptical polarization

J Daněk[1], M Klaiber[1], K Z Hatsagortsyan[1,3], C H Keitel[1], B Willenberg[2], J Maurer[2,3], B W Mayer[2], C R Phillips[2], L Gallmann[2] and U Keller[2]

[1] Max-Planck-Institut für Kernphysik, Saupfercheckweg 1, D-69117, Heidelberg, Germany
[2] Department of Physics, ETH Zurich, 8093, Zurich, Switzerland

E-mail: k.hatsagortsyan@mpi-k.de and jocmaure@phys.ethz.ch

Received 31 January 2018, revised 19 March 2018
Accepted for publication 28 March 2018
Published 14 May 2018

Abstract

We study strong-field ionization and rescattering beyond the long-wavelength limit of the dipole approximation with elliptically polarized mid-IR laser pulses. Full three-dimensional photoelectron momentum distributions (PMDs) measured with velocity map imaging and tomographic reconstruction revealed an unexpected sharp ridge structure in the polarization plane (2018 *Phys. Rev.* A **97** 013404). This thin line-shaped ridge structure for low-energy photoelectrons is correlated with the ellipticity-dependent asymmetry of the PMD along the beam propagation direction. The peak of the projection of the PMD onto the beam propagation axis is shifted from negative to positive values when the sharp ridge fades away with increasing ellipticity. With classical trajectory Monte Carlo simulations and analytical analysis, we study the underlying physics of this feature. The underlying physics is based on the interplay between the lateral drift of the ionized electron, the laser magnetic field induced drift in the laser propagation direction, and Coulomb focusing. To apply our observations to emerging techniques relying on strong-field ionization processes, including time-resolved holography and molecular imaging, we present a detailed classical trajectory-based analysis of our observations. The analysis leads to the explanation of the fine structure of the ridge and its non-dipole behavior upon rescattering while introducing restrictions on the ellipticity. These restrictions as well as the ionization and recollision phases provide additional observables to gain information on the timing of the ionization and recollision process and non-dipole properties of the ionization process.

Keywords: tunneling ionization, elliptical polarization, rescattering, non-dipole, Coulomb focusing cusp, laser magnetic field induced drift

1. Introduction

Recently, strong-field ionization in mid-IR laser fields has gained a lot of attention connected with the possibility of the production of coherent soft x-rays via high harmonic generation [1], and with the discovery of a variety of strong field phenomena, such as low-energy structures [2–4] and holographic electron interferences [5]. The concept of recollision and the related two-step model [6] provide a solid ground to attain a deeper insight into these types of processes. The simple two-step model proved to be so insightful because it catches the main feature of the dynamics: the recollision of the ionized electron during excursion in the laser field. This recollision is responsible for generating high-order harmonics [7, 8] or nonsequential double ionization [9–11]. However,

[3] Authors to whom any correspondence should be addressed.

the vast majority of the recolliding electrons undergoes elastic forward scattering with a small scattering angle. The omnipresent feature of elastic forward rescattering in photoelectron momentum distributions (PMDs) is described as Coulomb-focusing [12, 13], which is also the explanation for low-energy structures [2–4, 14–21]. From another perspective, the interference of forward rescattered electrons with different ionization paths leads to interferometric structures, such as electron-diffraction [22] and holographic interference structures [5].

Rescattering effects have been typically observed with linear polarization of the laser field, even though they exist and play a role also in the case of elliptical polarization [23–28]. The recollision signatures appear to be more pronounced when moving from the near-IR to the mid-IR laser fields, which can be explained by the following simple estimation. The Coulomb effect of the atomic core for the electron in the continuum can be described via rescatterings if the Coulomb field is significant only at the tunnel exit and at the recollision points. The latter requires that the electron quiver amplitude E_0/ω^2 largely exceeds the tunnel exit $\sim I_p/E_0$, as well as the recollision coordinates $\sim\Delta_\perp/\omega$. Here, E_0 and ω are the laser field amplitude and the angular frequency, respectively, I_p the ionization potential, and $\Delta_\perp = \sqrt{E_0}/(2I_p)^{1/4}$ the initial transverse momentum spread from the tunnel ionization theory [29, 30] (atomic units are used throughout). With the atomic charge number Z, the conditions above read $\gamma^2 \ll 1$, $\gamma\sqrt{E_0/E_a} \ll 1$, respectively [31]. Thus, the rescattering picture is valid for the tunneling regime of ionization, when the Keldysh parameter $\gamma = \omega\sqrt{2I_p}/E_0$ is small, $\gamma \ll 1$, and the laser field is small with respect to the atomic field $E_a = \kappa^3$, $E_0 \ll E_a$, with $\kappa = \sqrt{2I_p}$. Moreover, the increased quiver amplitude of the electron in these conditions facilitates multiple revisits to the ionic core. These conditions are strongly dependent on the laser parameters and more easily fulfilled in mid-IR long-wavelength laser fields. Therefore, the characteristic signatures of the recollision are expected to be significantly enhanced in the mid-IR laser fields.

Another important characteristic that changes by moving from near-IR to mid-IR wavelengths is the increased ponderomotive potential $U_p = {E_0}^2/4\omega^2$, which boosts the maximum kinetic energy of recollision, and in particular, allows keV harmonics [1], and laser induced electron diffraction with increased resolution [32]. In these conditions, the Lorentz force due to the laser magnetic field starts to significantly disturb the electron dynamics in the ionization process [33–38]. The role of the laser magnetic field (the leading non-dipole effect due to the vector potential inhomogeneity) for the recollision processes is characterized by the so-called Lorentz deflection parameter [39, 40]:

$$\Gamma_R \equiv \left(\frac{p_{zd}}{\Delta_\perp}\right)^2 = \gamma\frac{U_p^2}{\omega c^2}, \tag{1}$$

which is determined by the ratio of the averaged drift momentum along the laser propagation direction due to the laser magnetic field, $p_{zd} = U_p/c$, to the electron wave packet size in the momentum space $\Delta_\perp$ (or alternatively, by the ratio of the drift distance during the laser period to the electron wave packet size at the recollision [39, 41]). The Lorentz force along the laser propagation direction is responsible for the photon's momentum transfer to electrons observed in [42], and for the momentum partitioning between the ion and the electron during ionization [43–47]. The drift induced by the laser magnetic field is known to suppress the recollision and high-order harmonic generation at high laser intensities [33–36, 48–51], when $\Gamma_R \gtrsim 1$ ($I \gtrsim 10^{17}$ W cm^{-2} at a laser wavelength $\lambda = 800$ nm). Several methods, with tailored, focused, or counterpropagating laser pulses and additional fields, have been proposed to counteract the Lorentz drift and realize HHG in the weakly relativistic regime [52–63].

It is interesting to note that the recollision in the relativistic regime is not suppressed if a common atom is substituted by a positronium atom [64]. In this case both the electron and the positron have a similar drift and recollide coherently, leading to a concept of a high-energy microscopic laser collider [65–68], and to the vacuum laser collider [69–71].

At lower laser intensities, the magnetically induced drift is not large and recollisions are still possible, however, with a modified impact parameter in comparison to the dipole approximation case. The latter not only alters the recollision dynamics, but also has a back action on the electron drift properties along the laser propagation direction, i.e. the Coulomb focusing and the magnetically induced drift becomes interrelated, which was also noted in [72]. The first experiment, which demonstrates the modification of the Coulomb focusing in the non-dipole regime [73], revealed a counterintuitive shift of the peak of the projection of the PMD onto the beam propagation axis opposite to the beam propagation direction. The magnetic field induced lateral displacement of the electron and the successive recollision with the Coulomb potential is shown to cause this effect [73–75]. The role of the modified recollisions due to non-dipole effects in nonsequential double ionization has been discussed in [76].

In this paper we investigate the recollision process during strong field ionization in an elliptically polarized laser field at mid-IR wavelengths in the non-dipole regime. We investigate a sharp, thin line-shaped ridge structure of low-momentum electrons in the polarization plane first observed in [77] by analytical and numerical methods. We observe that it stems mainly from Coulomb-focused electrons undergoing multiple revisits of the parent ion with at least one significant rescattering event. The ridge position for longitudinal momenta corresponding to the slow recollision condition is at vanishing transverse momentum, whereas the ridge is bent for intermediate longitudinal momenta and is split at large ellipticities. For even larger ellipticities the ridge disappears. The appearance and disappearance of the sharp ridge structure is correlated with the non-dipole signatures of the PMD. In particular, the shift of the peak of the two-dimensional PMD with respect to the beam propagation axis is opposite to the beam propagation direction at small ellipticities and reversed into the beam propagation direction at larger ellipticities.

For the presented experimental conditions the non-dipole effects are expected to be small, because the Lorentz deflection parameter is small: $\Gamma_R \approx 0.006$. In terms of the photoelectron momentum shift, the non-dipole effect for the momentum component along the laser propagation direction is: $\delta p_z \sim \sqrt{\Gamma_R}\Delta_\perp \sim U_p/c \approx 0.03$ a.u. We were able to measure a momentum shift of this order and provide evidence of the leading non-dipole correction at nonrelativistic laser intensities.

The paper is organized as follows. The experimental results are presented in section 2. Section 3 is devoted to the theoretical analysis and the conclusion is given in section 4.

2. Experimental results

2.1. The setup

PMDs were recorded with a velocity map imaging spectrometer [78–80] with the gas nozzle integrated into the repeller to achieve high gas target densities in the interaction region [81, 82]. The target was ionized by an optical parametric chirped-pulse amplifier system based on chirped quasi-phase-matching devices. This system can deliver pulses with duration of 44 fs and pulse energy of 22 μJ at a center wavelength of 3.4 μm and a high repetition rate of 50 kHz [83, 84]. The pulses were focused with a backfocusing dielectric mirror with a focal length of 15 mm into the interaction region. The polarization of the laser beam was controlled by two custom-made achromatic MgF_2 wave plates. A quarter-wave plate induces the ellipticity and the subsequent half-wave plate controls the orientation of the polarization ellipse. The wave plates were fully characterized via polarimetry measurements where the power transmitted through a polarizer was recorded as a function of the angle between the major polarization axis and the polarizer axis. The polarization state at the desired orientation was extracted via a fit and interpolation of the measured values.

The intensity in all experiments was calibrated with reference measurements at close-to-circular polarization. The radial maximum of the torus-shaped momentum distribution was compared with classical trajectory Monte Carlo (CTMC) simulations [85].

Throughout the article, the following coordinate system will be used: the coordinate z denotes the direction of beam propagation, x the major and y the minor axis of the polarization ellipse and p_x, p_y, p_z the respective electron momenta. $W(p_x, p_y, p_z)$ denotes the PMD, i.e. the amplitude of the photoelectron signal.

The experiments require an accurate determination of the zero momentum spot, in particular on the beam propagation axis. This spot was identified via a sharp point in the center of the PMD, recorded with linear polarization that stems from the ionization of atoms that were left in a Rydberg state by the laser pulse and were subsequently ionized by the static electric field of the spectrometer [86, 87]. As these electrons do not interact with the pulse, they are guided by the static electric spectrometer field to the position on the detector that corresponds to zero momentum in the (p_x, p_z)-plane. The exact position of zero momentum in p_z-direction was determined from the projection of the PMD in a small range of 0.05 a.u. in p_x onto the p_z-axis. This projection was fitted with a Lorentzian profile. This method was applied analogously to find the center in p_x-direction.

2.2. Photoelectron momentum distributions

2.2.1. Photoelectron momentum distribution in the polarization plane. The 3D PMDs at various ellipticities at a laser intensity of 6×10^{13} W cm^{-2}, a pulse duration of 50 fs and a center wavelength of 3.4 μm are recorded to study the ellipticity dependence of rescattering in mid-IR laser pulses. When the ellipticity is varied, the electron dynamics changes mainly in the polarization plane, i.e. the (p_x, p_y)-plane. To have access to the polarization plane, we record the full 3D PMD from strong-field ionization, which is obtained by applying a tomographic reconstruction algorithm to the projected PMD measured with velocity map imaging [42, 88, 89]. The orientation of the 3D PMD with respect to the detector plane is linked to the orientation of the polarization ellipse, allowing us to rotate the PMD by rotating the polarization ellipse. The beam propagation axis is parallel to the detector plane. The polarization is rotated in steps of two degrees and a photoelectron image is recorded for each angular step. Subsequently, for each slice along the beam propagation direction, a filtered back-projection algorithm is applied for the tomographic reconstruction.

The ellipticity dependence of the PMDs in the polarization plane is shown in figure 1, see also [77]. Cuts of the 3D PMDs through the polarization plane (i.e. $W(p_x, p_y) = \int_{\Omega_z} W(p_x, p_y, p_z)\mathrm{d}p_z$) are shown in figure 1 for ellipticities of 0, 0.03, 0.07, 0.11, 0.15, 0.19, 0.23, 0.26. For the cuts we integrated over a range of $\Omega_z = \{|p_z| < 0.06 \text{ a.u.}\}$. The cuts show, that with increasing ellipticity, the ellipsoidally-shaped PMD evolves into a torus-like shape that is characteristic for strong field experiments with elliptically polarized pulses, as is typically observed for example with attoclock experiments [90, 91]. The appearance of the two maxima on the short axis of the polarization ellipse can be explained by a simple man's model [6]. Throughout this article, we will refer to the electrons ending in these maxima as type A electrons. Within the framework of this model, the maxima are shifted by 90° with respect to the phase at which the maximum of the electric field occurs. Deviations from 90° that are expected from the simple man's model are due to the Coulomb-interaction of the electron with the ion core [23, 85, 91], ionization delay times [90–93] and multi-electron effects like the induced dipole moment due to the ions polarizability [85].

In the evolution of the PMDs as a function of ellipticity, one can observe the appearance of a sharp, thin line-shaped ridge structure around $p_y = 0$ for small ellipticities, in particular for $\epsilon = 0.07$ and $\epsilon = 0.11$. To the best of our knowledge, no such sharp separated structure has been

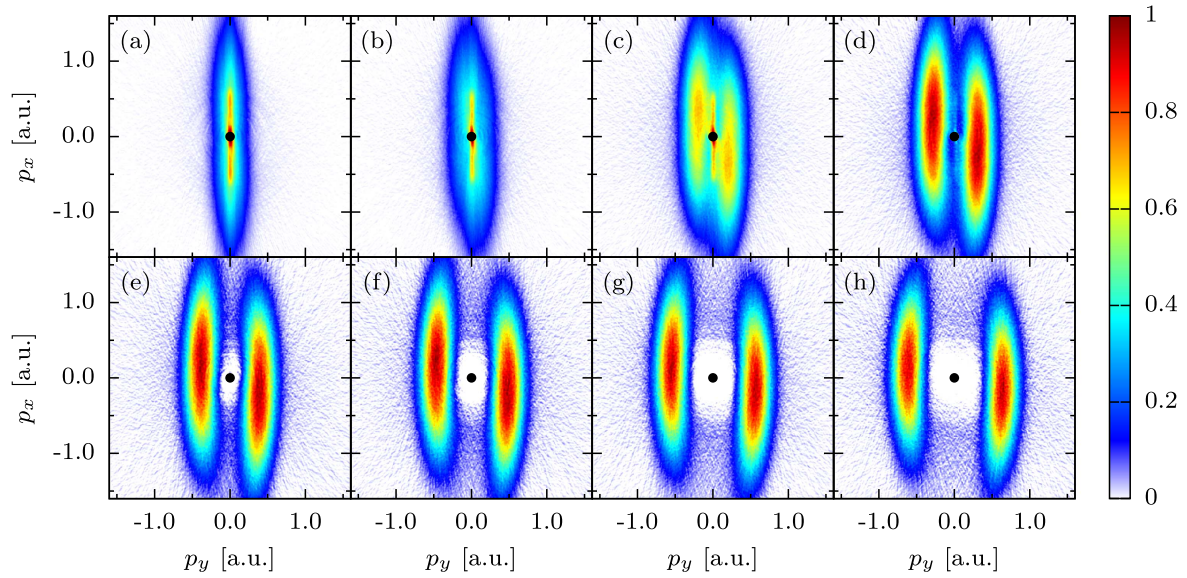

Figure 1. PMDs for xenon in the polarization plane measured at a peak intensity of 6×10^{13} W cm^{-2} for the ellipticities 0.0, 0.03, 0.07, 0.11, 0.15, 0.19, 0.23, 0.26, in (a)–(h), respectively. The central spot stemming from Rydberg states was cut out for illustration purposes. The shown PMDs are projections from the range $|p_z| < 0.06$ a.u. onto the polarization plane. The PMDs for ellipticities of $\epsilon = 0.07$ and $\epsilon = 0.11$ reveal a sharp line structure that disappears for larger ellipticities $\epsilon \geqslant 0.15$. The panels (a)–(f) were shown also in [77].

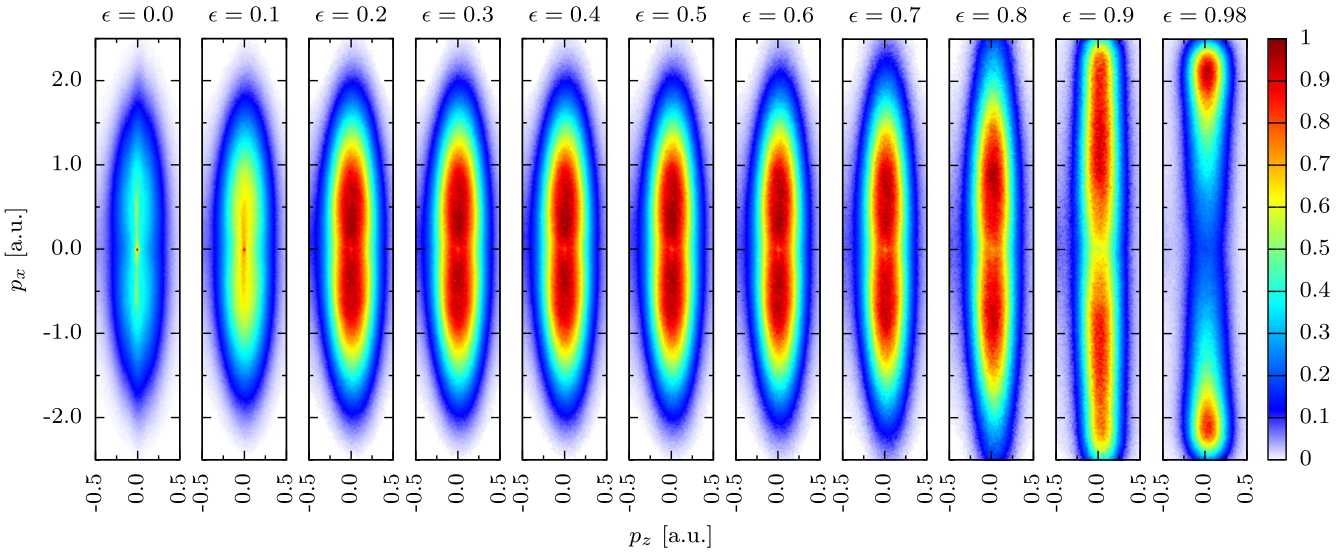

Figure 2. Normalized measured 2D PMDs from xenon recorded for various ellipticities at a peak intensitiy of 6×10^{13} W cm^{-2}.

observed in near-IR-experiments conducted at wavelengths around 800 nm in contrast to the study in the mid-IR presented here. For the rest of this article, we will refer to the electrons ending on the ridge as type B electrons.

2.2.2. Non-dipole effects. To investigate the interplay between Coulomb focusing, the ellipticity and the non-dipole effects, we performed ellipticity-resolved measurements of the drift induced by the laser magnetic field. Since our previous results [73] indicate that the non-dipole effects are independent of the target gas within the accuracy of our measurement, we perform our studies on a single species of atoms, xenon. The ellipticity was varied in steps from linear to close-to-circular ($\epsilon = 0.97$), see figure 2. For each ellipticity step, projected momentum images in the (p_x, p_z) plane were recorded. During the measurement we kept the intensity constant, not the electric field. Thus the total momentum transfer per cycle onto a free electron from the field is independent of the ellipticity. Figure 2 shows how the projected PMD is evolving from the typical cigar-like shape with the major dimension in p_x-direction towards a structure with maxima shifted to high values of p_x. Furthermore, the spot in the center stemming from Rydberg atoms ionized by the spectrometer field disappears with increasing ellipticity because the selection rules do not allow the excitation from the ground state into Rydberg states with circularly polarized light. Thus, reference measurements with

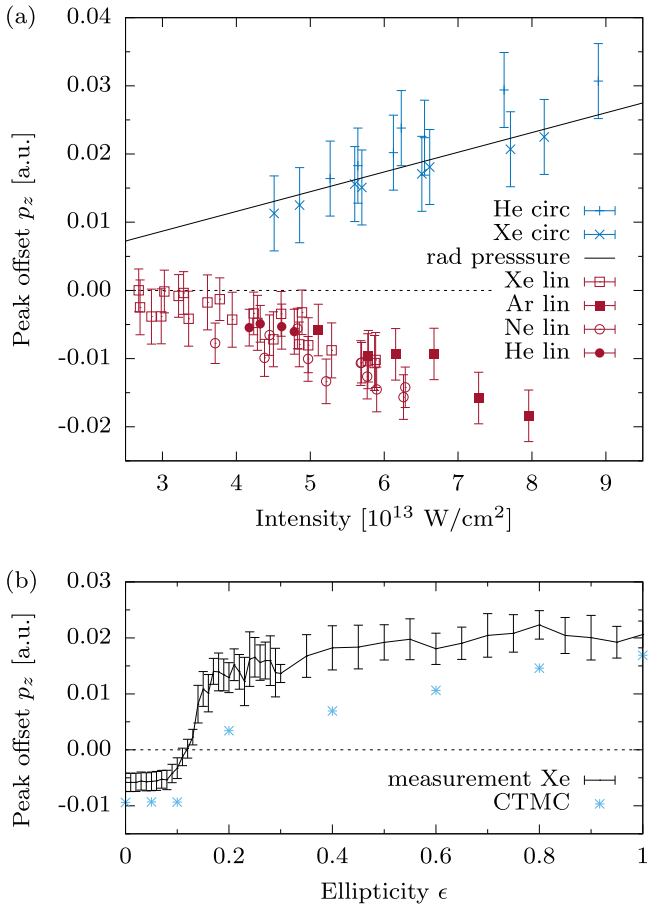

Figure 3. (a) Offsets of the peak of the PMDs projected onto the beam propagation axis (p_z) for circular polarization together with the data for linear polarization taken from [73]. We compare our data for circular polarization with the radiation pressure picture used in [87]. (b) Position of the peak of the PMD projected onto the p_z-axis as a function of ellipticity for a peak intensity of 6×10^{13} W cm^{-2}. We observe a transition from negative to positive values of p_z with the zero crossing at $\epsilon \approx 0.12$. The blue points in (b) are the results of CTMC simulations. The experimental points in the panel (b) were shown also in [77].

linear polarization were taken right before and after each ellipticity step. The peaks for reference zero were extracted in a similar fashion as the method applied in [73] and the one described in section 2.1. For each reference measurement, we recorded $N = 10$ photoelectron momentum images. The uncertainty of the determination of zero momentum scales with $\frac{1}{\sqrt{N}}$ due to N repetitive measurements that were weighted with the error of a Lorentzian fit of the peak of each projected distribution.

The peak of the projection was identified via a polynomial fit to the central part (i.e. $\Delta p_y \approx 0.05$ a.u.) of the PMD $W(p_z) = \int_\Omega W(p_x, p_y, p_z) \mathrm{d}p_x \mathrm{d}p_y$, with Ω being the integration momentum volume. The offset of that peak from $p_z = 0$ is shown in figure 3(b) as a function of the ellipticity. We observe an increase of the offset with increasing ellipticity from negative values (i.e. opposite to the beam propagation direction) to positive values (i.e. in beam propagation direction). The transition from negative to positive values occurs at an ellipticity of $\epsilon \approx 0.12$, which approximately corresponds to the ellipticity when the ridge structure in the PMD disappears, see figure 1.

We further proved the correlation of the ridge structure with the negative shift of the peak of the PMD along the laser propagation direction. Since we are able to isolate the electrons undergoing Coulomb-focusing in 3D momentum-space, type B electrons, we study their response separately from the mostly unfocused electrons for $\epsilon \approx 0.1$. We select type B electrons by choosing a narrow momentum range of $|p_y| < 0.05$ a.u. from the 3D PMD recorded at an ellipticity of $\epsilon = 0.11$. The electron signal that lies within this range and the electron signal from outside this range are separately projected onto the p_z-axis. The central spot stemming from ionization of Rydberg atoms was removed prior to the projections by ignoring the photoelectron signal with $|p| < 0.03$ a.u. The position of the peaks from A and B type electron signals in p_z-direction was identified. We observe that the type A electron signal peaks at a positive value of p_z and the type B electron signal at a negative value of p_z, see figure 3(c) in [77]. Thus, the ridge structure and correlated with it the non-intuitive behavior of the peak of the momentum along the laser propagation direction p_z at low ellipticities is connected with recollisions and Coulomb focusing.

In order to minimize the influence of rescattering processes, we also studied the projection of the PMD onto the beam propagation axis for the case of close-to-circular polarization for helium and xenon. We extract the zero momentum from reference images recorded with linear polarization as described in section 2.1. The peak position in p_z-direction of the projected PMDs for circular polarization was extracted via a Gaussian fit. The results for circular polarization are shown in figure 3(a) and they are consistent with the results from [87] within the error bars. Theoretical studies predicted an additional offset of the order of $I_p/3c$ at the tunnel exit [43] as well as in the final momentum distributions [44–46]. However, the experiment cannot resolve this additional offset. In addition, we show for comparison the data for linear polarization from [73] in the figure 3(a). In the case of linear polarization, the PMD peak is shifted opposite to the beam propagation direction in contrast to the data for circular polarization.

3. Theoretical analysis

3.1. The nature of the sharp ridge

To understand the nature of type A and B electrons, we have carried out CTMC simulations using the two-step model of strong-field ionization. The trajectories of the electrons are obtained by solving Newton's classical equations of motion in the electromagnetic field of the laser pulse and the Coulomb potential of the parent ion, using the initial conditions provided by the tunnel ionization theory in parabolic coordinates [29, 30, 85, 94]. Subsequently, the trajectories are binned in momentum space. The simulation results for the PMD in the polarization plane are shown in figure 4. Both

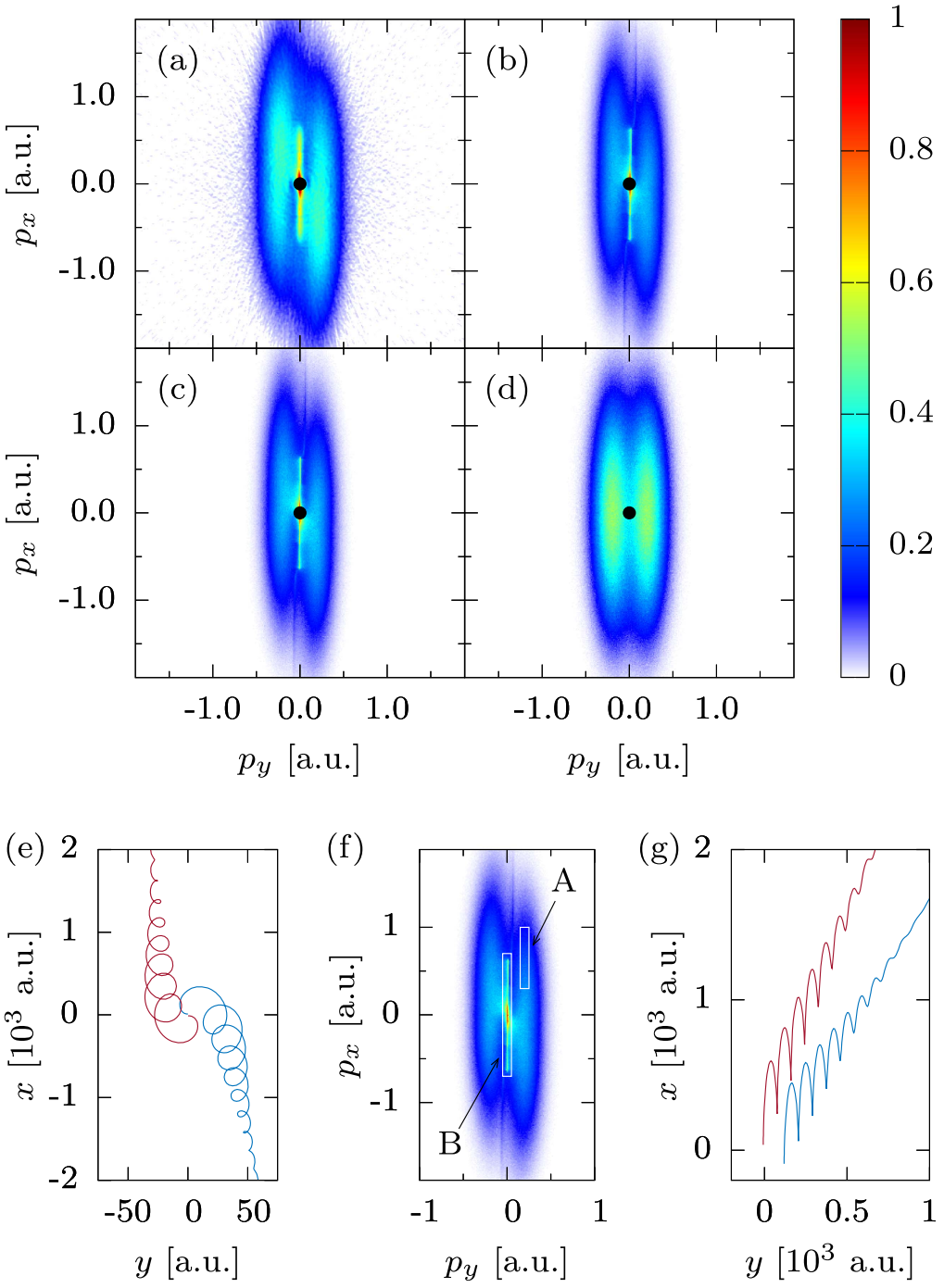

Figure 4. Comparison of experimental polarization plane PMDs with $|p_z| < 0.05$ a.u. (a) and corresponding CTMC calculations (b) from strong field ionization of xenon at an intensity of 6×10^{13} W cm^{-2}, a pulse duration of 50 fs and an ellipticity of $\epsilon = 0.07$. In both, the experimental data and the simulations, a sharp ridge appears around $p_y = 0$. (c) CTMC simulation where the Coulomb potential was included, but the magnetic field component was neglected. (d) CTMC simulation where the Coulomb potential was neglected, but the magnetic field component of the laser field was included. The sharp line around $p_y = 0$ disappears. (e) Characteristic trajectory (type B) from the central part of the PMD containing the focused photoelectrons. The trajectories revisit $x = 0$ multiple times and have a point of intersection in the (x, y)-plane. (f) The definition of the type A and B of trajectories. (g) Characteristic trajectory (type A) from the outer part of PMD, which goes directly to the detector without revisiting $x = 0$ and does not have a point of intersection in the (x, y)-plane. Each CTMC simulation used 10^8 trajectories.

type A and B electron signals are reproduced by the semi-classical treatment. The sharp ridge (type B electrons) is due to the Coulomb field of the atomic core, but not the laser magnetic field. In fact, it disappears in CTMC simulations when the Coulomb field is switched off, but stays unaltered when the magnetic field is removed, see figure 4. Type A and type B electrons have different characteristic trajectories as shown in figures 4(e)–(g). While type A electrons travel

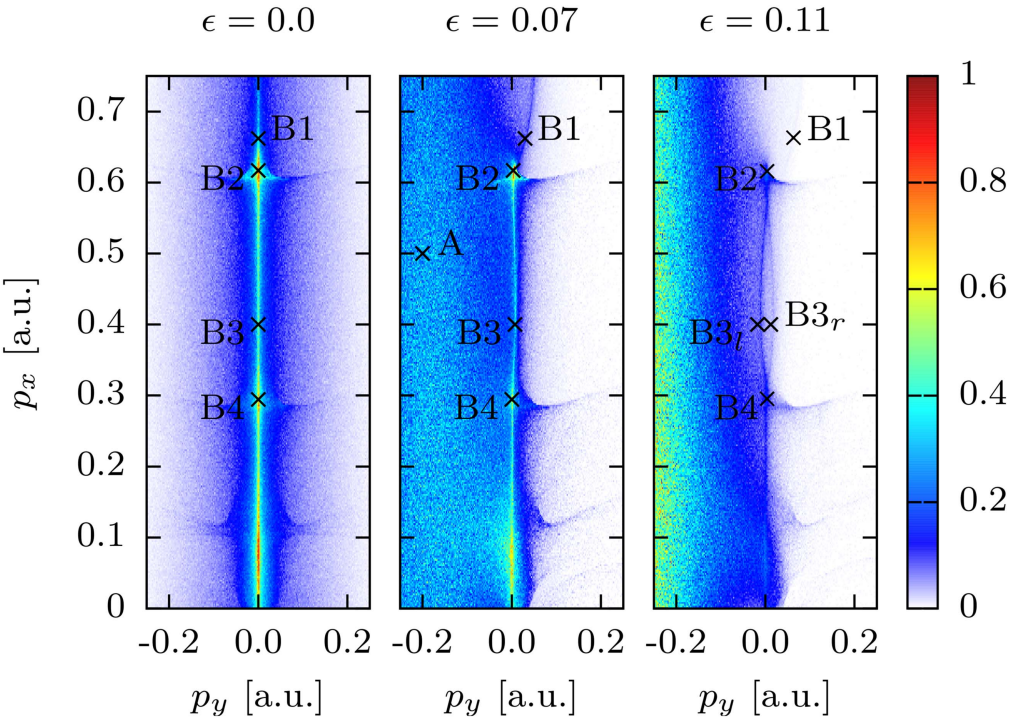

Figure 5. Comparison of central parts of the PMD ($|p_z| < 0.06$ a.u.), obtained by CTMC for different ellipticities: $\epsilon = 0$, $\epsilon = 0.07$ and $\epsilon = 0.11$, respectively. Characteristic points of the PMD depending on the specific longitudinal momenta, correspond in the linear polarization case, (B2) to the trajectory with two rescatterings, (B3) with three, (B4) with four rescatterings, and (B1) with a single rescattering. (B2) and (B4) correspond to the slow recollision condition ($p_{xr} = 0$). (A) corresponds to the center of the main lobe and is originating from recollision-free trajectories. Horizontal caustics are visible around, e.g. the characteristic points B2 and B4. Furthermore, a vertical caustic due to Coulomb focusing is visible as the line through the points Bn. For $\epsilon = 0.11$, the vertical caustic at point B3 is split. The dipole approximation is used in the CTMC simulations along with fixed CEP phase. The ionization is restricted to the central half-cycle of the laser pulse. The cases of $\epsilon = 0$ and 0.07 in the non-dipole regime were shown in [77].

directly to the detector without revisiting $x = 0$ (recollision), type B electron trajectories have a point of intersection in the (x, y)-plane and, furthermore, they cross $x = 0$ multiple times (multiple recollisions).

We continue our analysis to understand how recollisions appear in the elliptically polarized laser field and up to which ellipticities. The 3D PMD in the polarization plane (the (p_x, p_y)-plane) is calculated at different ellipticities $\epsilon = 0.07$ and 0.11, and compared with the case of linear polarization in figure 5. To focus on the mechanism of the creation of the ridge, we consider only electrons starting in the central half-cycle of the laser field to suppress the influence of ionization from multiple half cycles. Furthermore, we neglect the magnetic field effects to disentangle the creation of the ridge in the (p_x, p_y)-plane from additional effects in the beam propagation direction p_z.

The features of the PMD can be explained in the terms of laser-driven classical trajectories recolliding with the parent ion. In figure 5 we indicate several characteristic points exhibiting qualitatively different rescattering behavior. Point A is an example of a type A electron, while points Bn indicate type B electrons with n rescattering events. Due to the Coulomb interaction, a bunching of electrons occurs and is imprinted on the PMD in the form of caustics, see figure 5. There are two kinds of caustics: horizontal and vertical. Each horizontal caustic line in the PMD corresponds to the slow recollision, when the longitudinal momentum p_x of the electron at the recollision is vanishing (points B2 and B4 in figure 5). This condition depends on the ionization phase (i.e. the phase of the laser electric field when the electron appears in the continuum) and yields to longitudinal bunching of electrons [18].

In order to interpret the appearance of the vertical ridge, we analyze the set of initial transverse momentum distributions at the tunnel exit corresponding to the final transverse momentum values given by points Bn. The initial PMDs of corresponding points for linear and elliptical polarization are compared in figure 6. The ridge originates from a contraction of the transverse (with respect to the major polarization axis) momentum space of the ionized electron wave packet. In a linearly polarized laser field, the electrons contributing to the ridge are ionized with a nonvanishing transverse momentum at the tunnel exit, and appear after propagation with a vanishing transverse momentum. Their initial distribution is a ring in the (p_y, p_z)-initial transverse momentum distribution, see figure 6 left column. The electrons which are initially distributed inside this ring undergo hard recollisions and finally contribute either to the wings of the ridge or to high-energy region of the PMD, except for specific trajectories originating from the inner rings in figures 6(a)–(c). These electrons contribute to the center of the ridge due to multiple but well-balanced rescatterings (the Coulomb momentum

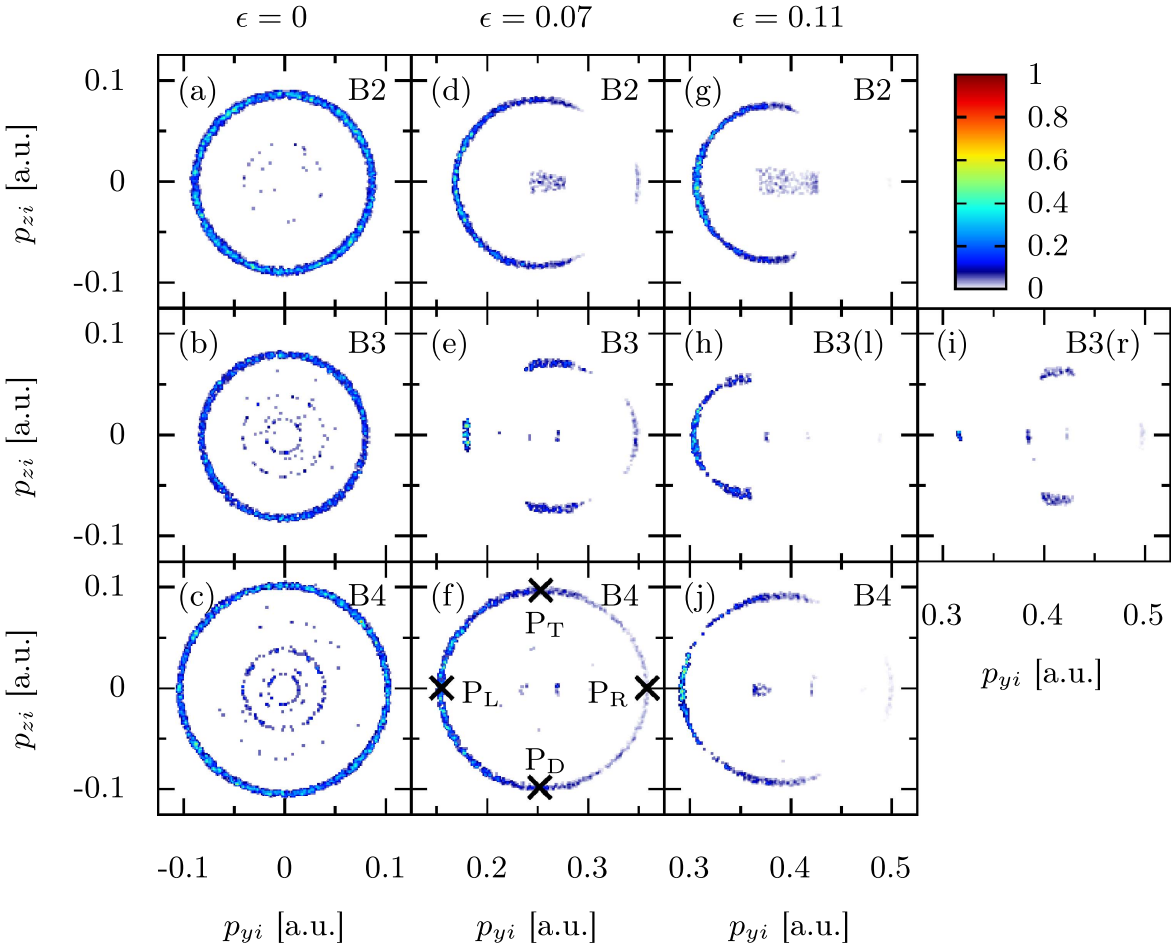

Figure 6. The initial momentum space distribution for trajectories ending in the momentum bins of 0.01 × 0.01 × 0.01 dimensions at the asymptotic values of longitudinal momentum p_x: (a) 0.62, (b) 0.44 and (c) 0.3 a.u., corresponding to the points B2, B3, B4 of figure 5, respectively. The laser field is linearly polarized in (first column), and elliptically polarized: with $\epsilon = 0.07$, in (second column), and $\epsilon = 0.11$, in (last two columns). Notice the positive offset in the p_{yi} of the structures in the right column due to the ellipticity. For $\epsilon = 0.11$ the ridge splits into two parts, represented by points B3(l) and B3(r) in panels (h) and (i), respectively. The pronounced left branch in (h) consists of electrons following linear-like trajectories, whereas the faint right branch comes from trajectories strongly influenced by the ellipticity. The points P_T, P_D, P_L, P_R are discussed in the text. In the CTMC simulations the dipole approximation is used along with fixed CEP phase and the ionization being restricted to the central half-cycle of the laser pulse. The cases of $\epsilon = 0$ and 0.07 in the non-dipole regime were shown in [77].

transfer to the electron changes the sign in consecutive rescatterings) strongly dependent on the electron initial conditions. The balance gets lost with the introduction of ellipticity, which manifest with suppression and eventual disappearance of the inner rings in figures 6(d)–(j).

In the case of the elliptically polarized laser field, there are two modifications to this picture. First of all, for small ellipticities (quantified in equation (17) below) the rescattering and Coulomb focusing, similar to the case of linear polarization, takes place for electrons which initially are distributed on a *shifted* ring of initial momenta in the (p_{yi}, p_{zi})-plane. The radius of the ring of the initial momentum space distribution is an indicator for Coulomb focusing. It is nearly the same for linear and elliptical polarization, i.e. Coulomb focusing for these trajectories is qualitatively the same. This type of electron trajectories contributes to the line-shaped ridge of the PMD in the case of elliptical polarization. The points B2 and B4 in figure 5 corresponding to the slow recollision condition do not change their position in the PMD when changing ellipticity, which is due to the similarity of the underlying trajectories. Secondly, at non-negligible ellipticities the type A electrons around vanishing initial transverse momentum have no recollision, no momentum change due to Coulomb field (besides the initial Coulomb momentum transfer as the electron leaves the tunnel exit), and contribute to the lobes of the final (p_x, p_y)-distribution. In contrast to the type B electrons, the initial momentum space of the type A electrons is a point, see figure 7, indicating the absence of Coulomb focusing (the initial and the final phase space are the same). In the case of $\epsilon = 0.07$ and $\epsilon = 0.11$ there are faint rectangle-like distributions inside the ring of the initial momentum distribution for B2, which are due to a new type of recolliding trajectories arising with increasing ellipticity. However, the number of these trajectories is not high, their contribution to the features of PMD is minor, and we do not discuss them further in the paper.

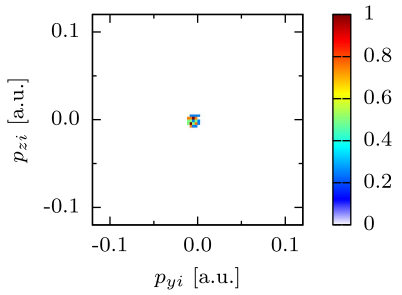

Figure 7. The initial momentum space distribution of direct electrons without Coulomb focusing which are ending in the center of the main lobe, point A in figure 5.

3.2. The structure of the sharp ridge

3.2.1. The shift of the initial momentum space of the ridge electrons. In this section we investigate the sharp ridge structure and its properties. First of all, let us determine initial momenta of the electrons at the tunnel exit which end up on the ridge. The initial transverse momentum space (p_{yi}, p_{zi}) of these electrons is a ring with a radius, which corresponds to the transverse momentum change due to Coulomb focusing [77]. In a linearly polarized laser field and in the dipole approximation the ridge is centered at $p_y = 0, p_z = 0$ in the final PMD due to the symmetry in the transverse momentum plane. The center of the initial momentum ring is at $p_{yi}^{(0)} = 0, p_{zi}^{(0)} = 0$. The ellipticity causes a momentum shift along the minor axis y, and the non-dipole effects induce a momentum shift of the cusp along the z-axis. In [76], such a shift in initial momentum was referred to as a momentum gate for double ionization that is imposed by the laser magnetic field and the recollision process.

In order to find these shifts, let us follow two electrons from opposite parts of the initial PMD-ring, which finally end up at the ridge with the same asymptotic momentum. For illustration, we mark such electrons in figure 6(f). At the beginning, we choose the left electron P_L with $p_{yi}^{-}, p_{zi} = 0$ and the right electron P_R with $p_{yi}^{+}, p_{zi} = 0$, which both have the same vanishing final momentum at the cusp:

$$p_{yf}^{-} = p_{yf}^{+}. \tag{2}$$

Using the solution of the electron equation of motion in the laser field, see equation (A5) in [77], and accounting for the Coulomb momentum transfer at the tunnel exit $\delta p_{yi}^{C\pm}$ and at the recollisions $\delta p_{yr}^{C\pm}$, we have for the final momentum

$$p_{yf}^{\pm} = -\epsilon \frac{E_0}{\omega} \cos\eta_i + p_{yi}^{\pm} + \delta p_{yi}^{C\pm} + \delta p_{yr}^{C\pm}, \tag{3}$$

where p_{yi} is the electron momentum at the tunnel exit, ϵ is the ellipticity, and η_i is the ionization phase. From equation (2) follows that the radius $R_{p_{yi}}$ of the ring in the initial momentum distribution is determined by the Coulomb momentum transfer:

$$R_{p_{yi}} \equiv \frac{p_{yi}^{+} - p_{yi}^{-}}{2} \approx \frac{\delta p_{yr}^{C-} - \delta p_{yr}^{C+}}{2}\left(1 + \frac{2E(\eta_i)}{(2I_p)^2}\right) \approx \delta p_{yr}^{C-}, \tag{4}$$

where we used $\delta p_{yi}^{C\pm} \approx -2p_{yi}^{\pm}E(\eta_i)/(2I_p)^2$ [31], $E(\eta_i) \ll E_a$, and $\delta p_{yr}^{C+} \approx -\delta p_{yr}^{C-}$. Taking into account that the center of the ridge is at $p_{yf} \approx 0$, we can find the initial momenta of the ridge electrons, i.e. the ellipticity induced recollision gate:

$$p_{yi}^{\pm} = \epsilon \frac{E_0}{\omega} \cos\eta_i - \delta p_{yi}^{C\pm} - \delta p_{yr}^{C\pm}. \tag{5}$$

The center of the ring is ellipticity dependent:

$$p_{yi}^{(\epsilon)} \equiv \frac{p_{yi}^{+} + p_{yi}^{-}}{2} \approx \epsilon \frac{E_0}{\omega} \cos\eta_i \times \left(1 + \frac{2E(\eta_i)}{(2I_p)^2}\right) \approx \epsilon \frac{E_0}{\omega} \cos\eta_i. \tag{6}$$

Thus, in the case of elliptical polarization the ring of the initial momentum distribution for the sharp ridge electrons is shifted due to the elliptical drift momentum along the minor axis of polarization. Similar to the ring radius $R_{p_{yi}}$, the initial momenta of the ridge electrons can be expressed via the Coulomb momentum transfer at the recollisions:

$$p_{yi}^{\pm} = p_{yi}^{(\epsilon)} \pm R_{p_{yi}} \approx \left(\epsilon \frac{E_0}{\omega} \cos\eta_i \pm \delta p_{yr}^{C-}\right) \times \left(1 + \frac{2E(\eta_i)}{(2I_p)^2}\right). \tag{7}$$

The indicator of Coulomb focusing is the radius of the ring $R_{p_{yi}}$ in the initial transverse phase space distribution, which according to equation (4) is determined by the Coulomb momentum transfer at recollisions. We have calculated the Coulomb momentum transfer numerically for specific trajectories in figure 8. It is determined as the difference of the exact numerical solution for the momentum component $p_y^{\text{num}}(\eta)$ and that in the laser field, given by equation (A5) of [77]:

$$\delta p_y^{C}(\eta) \equiv p_y^{\text{num}}(\eta) - [A_y(\eta) - A_y(\eta_i) + p_{yi}], \tag{8}$$

with the ionization phase η_i, and the corresponding initial momentum p_{yi}. As we can see the Coulomb momentum transfer at recollisions for all three points B2, B3, B4 is approximately the same as in the case of linear polarization. Therefore, the radii of the rings and Coulomb focusing are also the same.

The magnetically induced drift shifts the initial momentum distribution for the sharp ridge electrons along the z-axis. To show this, let us first calculate the final momentum along the laser propagation direction. According to equation (A11) of [77],

$$p_{zf} = p_{zi} + p_{zd}^{(i)} + \delta p_{zi}^{C} + \delta p_{zr}^{C}, \tag{9}$$

where $p_{zd}^{(i)} \equiv \frac{A^2(\eta_i)}{2c} - \mathbf{p}_i \cdot \frac{\mathbf{A}(\eta_i)}{c}$. The Coulomb momentum transfer at the recollision can be estimated [31]:

$$\delta p_{yr}^{C} \approx -\frac{y_r}{R_r^3}\delta t_r, \tag{10}$$

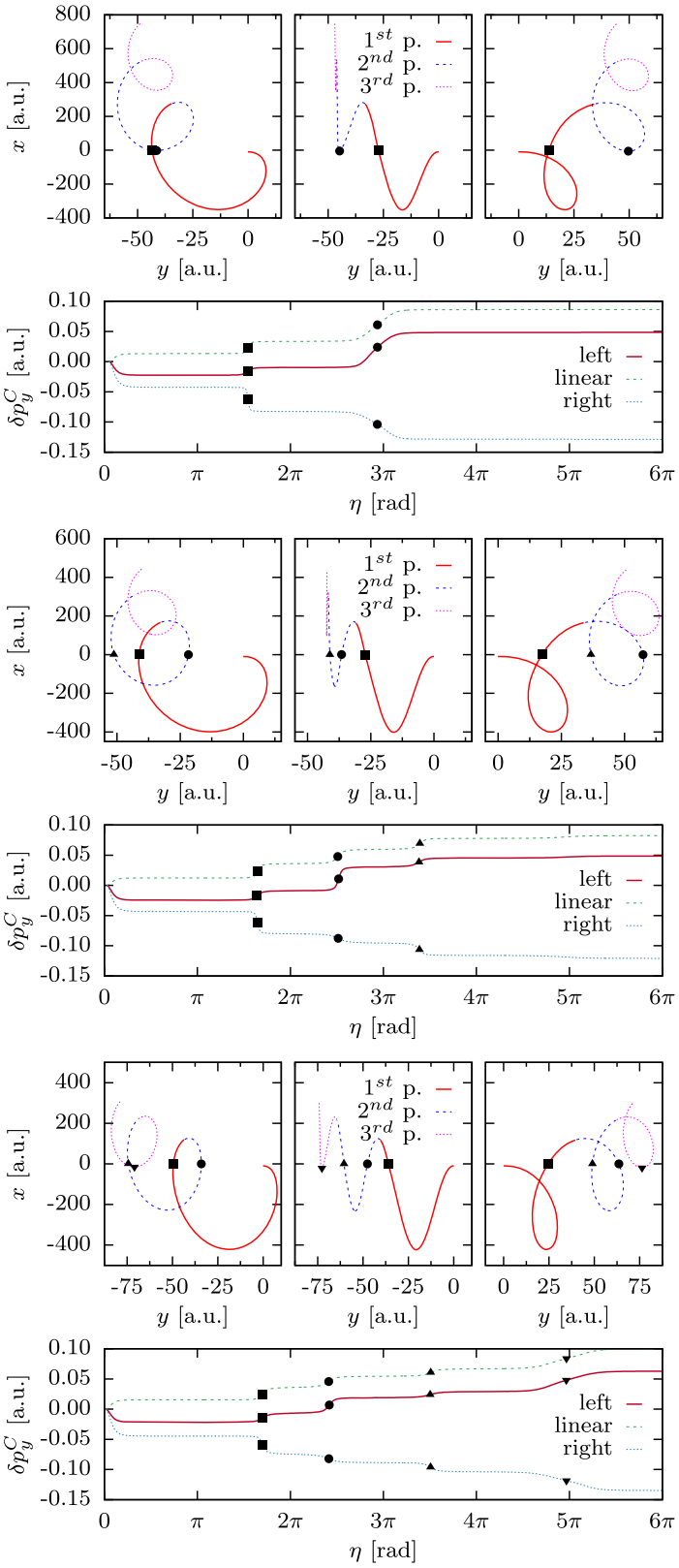

Figure 8. Typical photoelectron trajectories in a laser field with $\epsilon = 0.07$, as well as initial Coulomb momentum transfer and Coulomb momentum transfer during recollision. The trajectories originate on the left (left panels) and right part (right panels) of the initial transverse momentum distribution ring with $p_{zi} = 0$ and end up at the same point B2 (upper group), B3 (middle group), and B4 (bottom group). The middle panels of trajectories show the case of linear polarization. The slow recollisions are the second one in B2, and the forth one in in B4. In left panels the slow recollisions have the same impact parameters (y-coordinate) as in the linear polarization case (middle panel).

$$\delta p_{zr}^{C} \approx -\frac{z_r}{R_r^3}\delta t_r = \frac{z_r}{y_r}\delta p_{yr}^{C}, \tag{11}$$

where y_r, z_r, and R_r are the recollision coordinates and the recollision distance, respectively, and δt_r is the recollision duration. As we analyze the case $p_{zi} = 0$, the electron trajectory in the laser field via equations (A16) and (A17) of [77] is

$$\begin{aligned} y_r &= \left(\epsilon\frac{E_0}{\omega}\frac{\sin\eta_r - \sin\eta_i}{\eta_r - \eta_i} + p_{yi} + \delta p_{yi}^{C} - \epsilon\frac{E_0}{\omega}\cos\eta_i\right) \\ &\quad\times (t_r - t_i) \approx \left(p_{yi} + \delta p_{yi}^{C} - \epsilon\frac{E_0}{\omega}\cos\eta_i\right)(t_r - t_i) \\ &= -\delta p_{yr}^{C}(t_r - t_i) \\ z_r &= (\overline{p}_{zd} + \delta p_{zi}^{C})(t_r - t_i), \end{aligned} \tag{12}$$

where $\overline{p}_{zd} \equiv \frac{1}{2c}\int_{\eta_i}^{\eta_r}[\mathbf{A}(\eta') - \mathbf{A}(\eta_i)]^2\frac{\mathrm{d}\eta'}{\omega} + \frac{1}{c}\int_{\eta_i}^{\eta_r}\mathbf{p}_i\cdot[\mathbf{A}(\eta') - \mathbf{A}(\eta_i)]\frac{\mathrm{d}\eta'}{\omega}$. In the second line we have taken into account the condition for the ridge electron from equation (5), as well as neglected the first term in the brackets (it vanishes at the slow recollision condition $p_{xr} \approx 0$, i.e. at $\sin\eta_r \approx \sin\eta_i$, see equation (A4) in [77], and it is also small otherwise due to the relatively large $\eta_r - \eta_i$). As a consequence, we can conclude from the second expression of equation (11) that in the case of $p_{zi} = 0$,

$$\delta p_{zr}^{C} \approx -\overline{p}_{zd} - \delta p_{zi}^{C}, \tag{13}$$

and from equation (9) the z-component of the final momentum of the ridge electrons is

$$p_{zf} \approx -\overline{p}_{zd} + p_{zd}^{(i)}. \tag{14}$$

Further, let us consider another electron pair in the initial momentum distribution ring, marked as either $\mathrm{P_T}$ or $\mathrm{P_D}$ in figure 6(f). As it belongs to the sharp ridge with the same final momentum as in equation (14), we can use equations (9) and (14) to find the z-component of its initial momentum, i.e. the laser magnetic field induced recollision gate:

$$p_{zi} = -\overline{p}_{zd} - \delta p_{rz}^{C} - \delta p_{iz}^{C}, \tag{15}$$

while in the dipole limit it is $p_{zi} = -\delta p_{rz}^{C} - \delta p_{iz}^{C}$, i.e. the non-dipole effects shift the initial distribution ring for the sharp ridge electrons by $-\overline{p}_{zd}$ in the z-direction.

The comparison with the linear polarization case reveals, that the ellipticity induced shift of the initial momentum distribution corresponding to the ridge electrons dominates over the non-dipole induced shift in the considered parameter regime, compare figures 6(g)–(j) with figures 4(a)–(c) of [77].

The sharp ridge due to recollisions will exist if the required initial transverse momentum of type B electrons according to equations (5) and (15), is within the momentum width of the tunneled electron wave packet $\Delta_\perp$. For the present laser parameters $p_{zd}/(E_0/\omega) \sim 10^{-2}$. Then, the condition above reads

$$\epsilon\frac{E_0}{\omega} \lesssim \Delta_\perp. \tag{16}$$

From the latter we conclude that the ridge in the PMD can exist up to ellipticities

$$\epsilon \lesssim \frac{\omega}{\sqrt{E_0}\,(2I_p)^{1/4}} \approx 0.07. \tag{17}$$

There are modifications of the rings in figure 6 due to ellipticity, especially for B3, which we discuss in the next section based on trajectory analysis. Note that the inner rings in the linear case in figure 6 are caused by trajectories with multiple significant rescattering events, which are strongly suppressed at increasing ellipticity. At larger ellipticities, when the sharp ridge disappears, the recollision effect is negligible assuming that the electron final momentum component along the laser propagation direction is positive and determined by the non-dipole drift momentum of free electrons: $p_{zf} = p_{zd}^{(i)}$. We compare the CTMC simulations for the peak of the PMD projection onto the p_z-axis as a function of ellipticity with the experimental results in figure 3(b). Qualitatively the CTMC simulations reproduce the experimentally observed trend of the peak position as a function of ellipticity. The quantitative discrepancy at low ellipticities can be explained by focal volume averaging, not included in the simulation.

3.2.2. The ridge modification with respect to the linear polarization case. Next, we analyze the modifications of the ridge as a function of ellipticity. For the points B2 and B4 and linear polarization the main Coulomb momentum transfer during recollision takes place at the slow recollision, $p_{xr} = 0$. This corresponds to the second recollision for B2 and the fourth near B4. Although there are multiple recollision points, $x_r = 0$ (two at B2, and four at B4, see figure 8), the Coulomb momentum transfer is the largest at the slow recollision in both cases. In the elliptical polarization case, the Coulomb focusing for the trajectory coming from the left part of the ring resembles the linear case, since the slow recollision has the same impact parameter and the same Coulomb momentum transfer during recollision. Of the multiple recollisions that occur for these points, the slow one has the dominant effect on the final momentum, especially for elliptical polarization (figure 8). This is because at elliptic polarization the impact parameter for the fast recollisions is larger than for linear polarization due to the oscillating part of the y-coordinate. Therefore, the Coulomb focusing for the left half-ring in figure 6 (the ring radius) is the same for both linear and elliptical polarizations, thereby creating the central ridge in the PMD in both cases.

In contrast, the trajectory from the right part of the ring at B2 in the elliptical polarization case differs from the linear one, see figure 8, upper right panel. The first rescattering for this trajectory, additional to the slow recollision, takes place with smaller impact parameter than in the linear case due to the oscillating part of the y-coordinate, resulting in an increase of the total Coulomb momentum transfer. This explains the larger radius of the right half-cycle of the ring structure at B2 in figure 6. The right-type trajectories are more sensitive to the initial conditions and, consequently, the ring width is significantly smaller. Moreover, the ionization probability is

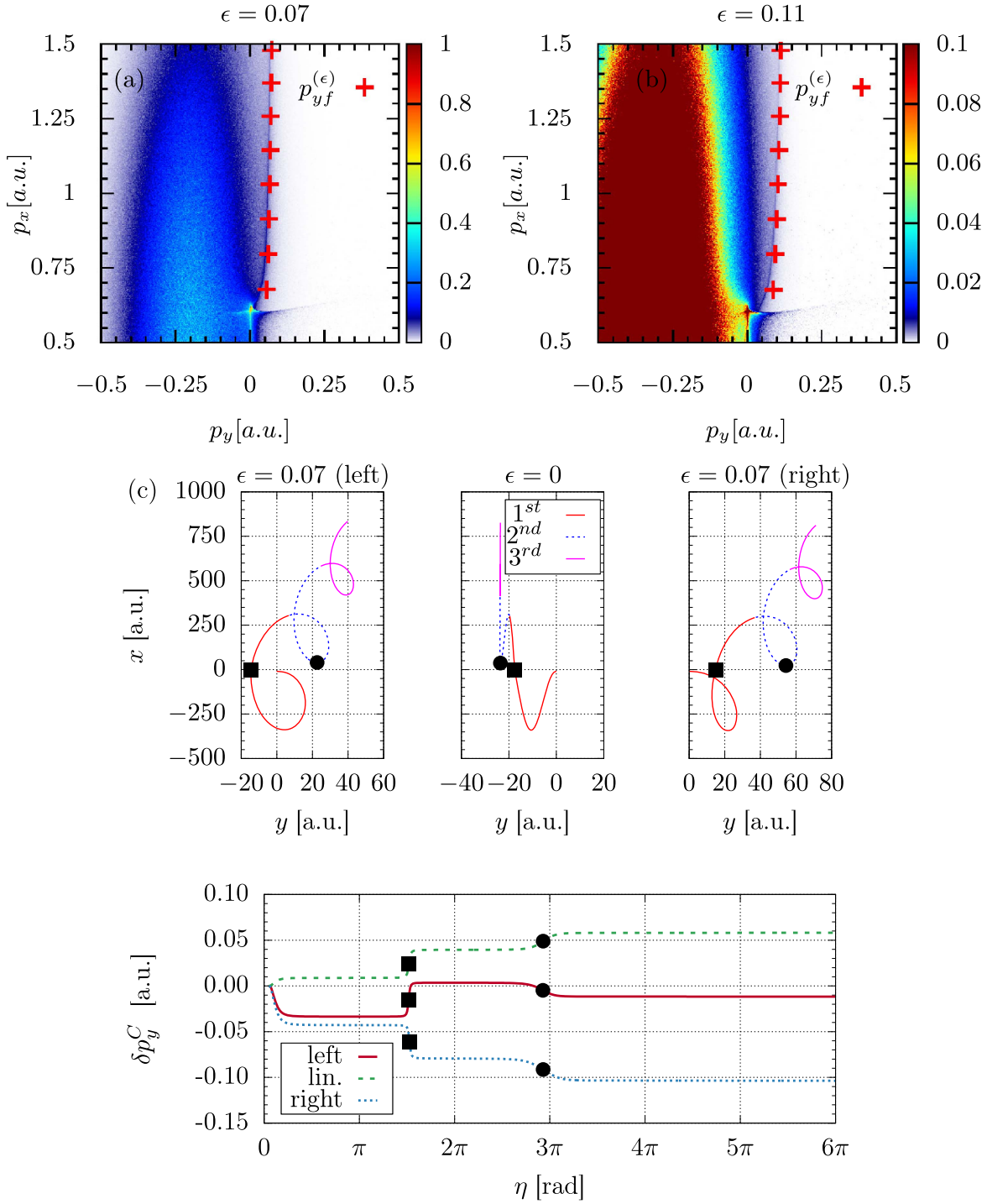

Figure 9. The bent central ridge above the point B2: the comparison of the CTMC simulations with the estimation of the deflected momentum $p_{yf}^{(\epsilon)}$ from equation (25) for (a) $\epsilon = 0.07$ and (b) $\epsilon = 0.11$, respectively; (c) typical photoelectron trajectories in a laser field with $\epsilon = 0.07$, as well as the initial Coulomb momentum transfer and that at recollision. The trajectories originate on the left (left panels) and right part (right panels) of the initial transverse phase space distribution ring with $p_{zi} = 0$ and end up at the same point B1. The middle panel of trajectories show the case of a linear polarization.

smaller for the right part of the ring because of the larger initial momenta. This explains why the central ridge becomes less pronounced with increasing ellipticity.

However, the right trajectories for B4, and trajectories ending up on the central ridge at $|p_x|$ smaller than for B4, start to resemble the linear case again. This is because for the ionization phases that are relevant to these trajectories, the oscillating part of the y-coordinate does not perturb the recollision coordinates significantly. The condition for this is

$$|y_r^{(\epsilon)} - y_r^{(0)}| \ll y_r^{(0)}, \tag{18}$$

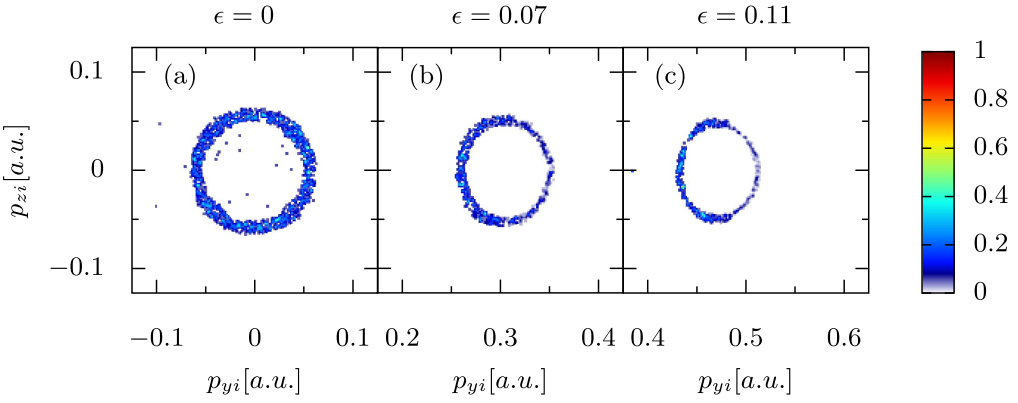

Figure 10. The initial transversal phase spaces for $\epsilon = 0$, $\epsilon = 0.07$, and $\epsilon = 0.11$ respectively, resulting in trajectory with a single rescattering event at B1. The ellipticity shifts the initial transverse momentum ring in the p_y-direction and causes a slight deformation.

with the index $^{(0)}$ indicating the linear polarization, from which we can estimate the threshold ionization phase. Using equations (A25) and (A32) of [77], and the approximations $\eta_r^{(\epsilon)} = \eta_r^{(0)}$ and $\eta_i^{(\epsilon)} = \eta_i^{(0)}$, this condition reads

$$\left| \epsilon \frac{E_0}{\omega^2}(\sin\eta_r - \sin\eta_i) \right| \ll (p_{yi}^{(0)} + \delta p_{yi}^{C(0)}) \frac{(\eta_r - \eta_i)}{\omega}, \quad (19)$$

which can be expressed via the Coulomb momentum transfer at the recollision δp_{yr}^C:

$$|\sin\eta_r - \sin\eta_i| \ll \frac{\delta p_{yr}^C}{(\epsilon E_0/\omega)}(\eta_r - \eta_i). \quad (20)$$

The recollision phase is found from the condition $x(\eta_r) = 0$. Taking into account that for the first recollision $\eta_r \approx 2\pi - \eta_r'$, with $\eta_r' \ll 1$, we find

$$\eta_r' \approx \sqrt{4\pi\eta_i}, \quad (21)$$

and the condition of equation (20), at which the oscillating part of the y-coordinate does not perturb the recollision coordinates significantly, reads

$$\eta_i \ll \pi \left(\frac{\delta p_y^C}{(\epsilon E_0/\omega)} \right)^2 \approx 0.7, \quad (22)$$

for $\delta p_y^C = 0.1$, $\epsilon = 0.07$, and the laser parameters of the experiment $E_0 \approx 0.04$, $\omega \approx 0.013$. The latter means that at $\eta_i \lesssim 0.07$, which assumes $p_x \lesssim E_0\eta_i/\omega \approx 0.2$, the recollisions and Coulomb focusing in the elliptical polarization case will be similar to the linear one. This estimation fits to the CTMC calculation in figure 5.

The ring of the initial momenta of point B3 is deformed in a stronger way than the one for B2. The deformation is due to the fact that both left and right trajectories are perturbed with respect to the linear polarization case because of the quiver motion in the transversal y-direction. The perturbed trajectories are more sensitive to the initial conditions, which results in a variable width of the ring in the initial momentum distribution. Moreover, the recollision coordinates for both left and right trajectories are different. Therefore, the Coulomb momentum transfer during recollision for the left and right trajectories are not symmetric which leads to the bend of the central ridge. Furthermore, at larger ellipticities, e.g. $\epsilon = 0.11$, the central ridge at B3 is split, when the left- and right-side trajectories yield to different ridges B3(r) and B3(l), respectively, see figures 6(h)–(i). However, this splitting is not visible in the experimental data due to focal volume averaging, CEP averaging and the laser pulse envelope.

Above the point B2, when the photoelectrons rescatter once only, the ridge is bent, see figure 9, i.e. the final p_y-momentum is nonvanishing. The reason one can deduce by looking at the left trajectory for point B1 in figure 9(c). We can ignore the role of the second rescattering, since its importance diminishes with increase of the final longitudinal momentum, and assume the first rescattering only. For the single rescattering trajectories above the point B2, the rescattering coordinate is very similar to the linear polarization case. In the example presented in figure 9, the electrons from both sides of the initial momentum distribution ring ionized with the same phase η_i recollide at the same phase η_r and with the same impact parameter, i.e.

$$y_r^{(\epsilon)-} = -y_r^{(\epsilon)+}. \quad (23)$$

The latter is ensured by proper values of $p_{yi}^{(\epsilon)-}$ and $p_{yi}^{(\epsilon)+}$ which can compensate for the transversal dynamics introduced by the ellipticity and hence lead to the same absolute value of Coulomb momentum transfer for the opposite trajectories with analogy to the linear case. From the condition of equation (23), and by using equation (A25) of [77] with $y_i = 0$, we derive the momentum of the center of the initial momentum ring of the ridge electrons presented in figure 10:

$$p_{y0}^{(\epsilon)} \equiv \frac{p_{yi}^{(\epsilon)-} + p_{yi}^{(\epsilon)+}}{2} = \delta\bar{p}_{yi}^{C(\epsilon)} + \epsilon \frac{E_0}{\omega}\left(\cos\eta_i - \frac{\sin\eta_r - \sin\eta_i}{\eta_r - \eta_i} \right), \quad (24)$$

where we have defined the averaged initial Coulomb momentum transfer for the ring's center as $\delta\bar{p}_{yi}^{C(\epsilon)} \equiv \frac{1}{2}(\delta p_{yi}^{C(\epsilon)-} + \delta p_{yi}^{C(\epsilon)+})$. The final momentum of the ridge in

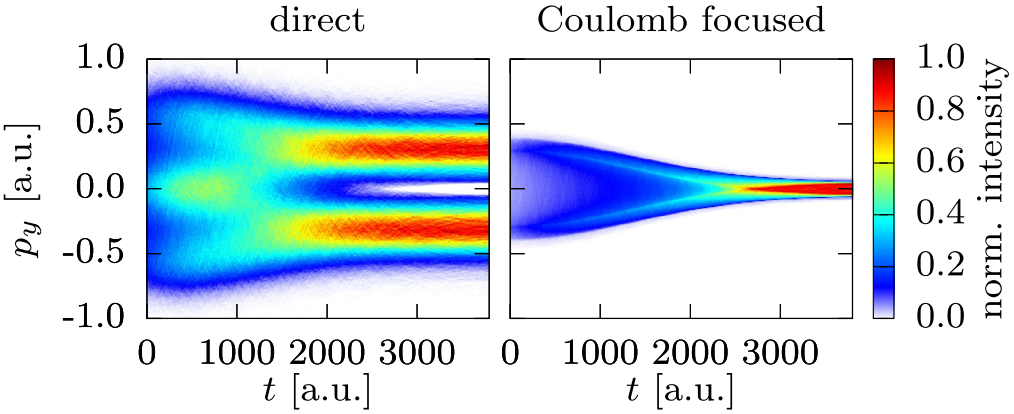

Figure 11. Momentum spread as a function of time for direct and Coulomb-focused electrons with CTMC simulations using the two-step model of strong-field ionization with adiabatic tunneling theory and both electric and magnetic field included for an ellipticity of $\epsilon = 0.11$. Coulomb-focused rescattered electrons end up in the ridge and the direct electrons in the lobes of the 3D PMD.

this case equals:

$$p_{yf}^{(\epsilon)} = p_{y0}^{(\epsilon)} - \epsilon \frac{E_0}{\omega} \cos \eta_i - \delta \bar{p}_{yi}^{C(\epsilon)}$$
$$= -\epsilon \frac{E_0}{\omega} \left(\frac{\sin \eta_r - \sin \eta_i}{\eta_r - \eta_i} \right). \quad (25)$$

The estimation of $p_{yf}^{(\epsilon)}$ is plotted in figure 9 and shows agreement with the simulations. Only a slight discrepancy appears near the point B2 which is caused by the omission of the second recollision which yields additional momentum transfer further diminishing $p_{yf}^{(\epsilon)}$. Moreover, the $p_{yf}^{(\epsilon)}$ is positive for all single recollision trajectories and vanishes for linear polarization as expected.

4. Conclusion

With a detailed analysis, we identified a subspace in the momentum representation of the tunnel ionized electron wave packet, which in an elliptically polarized laser field shows recollision dynamics similar to the linear polarization case. The electron trajectories originating in this initial PMD subspace have multiple revisits, including at least one significant rescattering event with the parent ion, which causes the large initial momentum subspace to be squeezed into a small final momentum space having near vanishing transverse momentum. The effect occurs due to Coulomb focusing, and leads to the creation of the sharp ridge structure in the momentum space for linear as well as for elliptical polarization. Thanks to this feature, we are able to separate the electrons that experienced strong Coulomb focusing in momentum space from the unfocused electrons in the case of elliptical polarization, see figure 11. The final momenta of Coulomb-focused electrons that underwent slow recollisions, and hence experienced strong Coulomb focusing, are almost unaltered by the introduction of a small ellipticity. The main difference for elliptical polarization with respect to the linear case is in fact the change of the starting condition of the electrons that end up in the ridge. The ellipticity causes a shift of the initial momenta of the ridge electrons along the minor axis of polarization, and the non-dipole effects induce a shift along the laser propagation direction. The same message is formulated in [76] in terms of gating: the recollision and the magnetic field combined act as a gate. While in the latter the gate imposes a restriction on the initial momenta of the ionized electron to realize nonsequential double ionization, here we relate the non-dipole and ellipticity gating to the soft recollisions and Coulomb focusing. The focus of [76] is the asymmetry of the whole PMD, but we concentrate mostly on the peak of the PMD, investigating the Coulomb focusing cusp and its properties.

We investigated the modifications and the structure of the Coulomb focusing ridge as a function of the ellipticity of the laser field. The ridge is bent and split at longitudinal momenta deviating from the slow recollision conditions. We trace these properties of the ridge in the modification of the electron recollision properties in an elliptically polarized laser field with respect to the linear polarization case. Unfortunately, the fine structure of the ridge obtained in CTMC simulations is not visible in the experimental spectra due to focal volume and CEP averaging, and the laser pulse envelope.

We also learned that the central part of the tunnel ionized electron wave packet in momentum space provides unfocused electrons which are steered away by the elliptical polarization into ellipsoidal shaped side lobes of the final PMD. We use the full 3D PMD to study the different non-dipole response for both type of electrons with and without strong Coulomb-focusing. The separation of the electron trajectories allows us to disentangle the response of the different photoelectrons to non-dipole effects and to make the connection between prior results of Ludwig *et al* [73] and Smeenk *et al* [87]. In [87], a shift of the PMD in beam propagation direction was reported and a simple radiation pressure picture was used as an explanation. In [73], the peak of the projection of the PMD was shifted opposite to the beam propagation direction. Here, we were able to experimentally isolate the electrons that are responsible for this counterintuitive shift and to separately study their non-dipole response. We observed an ellipticity dependent offset of the position of the peak of the projection of the PMD on the beam propagation axis. By increasing the

ellipticity from linear to circular, this offset shifts from negative to positive values of p_z. The appearance of a peak on the negative or positive side of $p_z = 0$ can be considered as a competition of the type A (direct) and type B (Coulomb-focused) electrons. In case that the peak is formed mainly by type A electrons, the projection of the PMD peaks at positive values of p_z whereas in the case that the type B electrons dominate the peak of the projected PMD, it is shifted towards negative values of p_z. Thus, Coulomb focusing has an essential influence on non-dipole effects, creating a non-trivial dependence of the PMD shift along the laser propagation direction on the ellipticity of the laser field. Our results open up new possibilities to study the photoelectrons experiencing strong rescattering separately from the direct electrons and the electrons that experience only weak Coulomb interaction.

We obtained an analytical relationship between the initial momentum of the ridge electrons, the drift momentum of the electron due to ellipticity and due to non-dipole effects, and the Coulomb momentum transfer upon recollision, which allowed us to identify the range of ellipticity for which the ridge appears. These findings can be exploited to gain additional information on the timing of the ionization and recollision process as well as on wave packet properties.

Acknowledgments

This research was supported by the NCCR MUST, funded by the Swiss National Science Foundation and by the ERC advanced grant ERC-2012-ADG_20120216 (ERC ADG AttoClock—320401) within the seventh framework programme of the European Union. BW was supported by an ETH Research Grant ETH-11 15-1.

ORCID iDs

J Daněk https://orcid.org/0000-0002-0017-3804
K Z Hatsagortsyan https://orcid.org/0000-0002-1407-9122
C H Keitel https://orcid.org/0000-0002-1984-1470
B Willenberg https://orcid.org/0000-0002-6822-951X
J Maurer https://orcid.org/0000-0001-8003-1015
C R Phillips https://orcid.org/0000-0001-5307-153X
L Gallmann https://orcid.org/0000-0003-3167-8271
U Keller https://orcid.org/0000-0002-1689-8041

References

[1] Popmintchev T *et al* 2012 *Science* **336** 1287–91
[2] Blaga C, Catoire F, Colosimo P, Paulus G, Muller H, Agostini P and DiMauro L 2009 *Nat. Phys.* **5** 335–8
[3] Quan W *et al* 2009 *Phys. Rev. Lett.* **103** 093001
[4] Wolter B, Pullen M G, Baudisch M, Sclafani M, Hemmer M, Senftleben A, Schröter C D, Ullrich J, Moshammer R and Biegert J 2015 *Phys. Rev.* X **5** 021034
[5] Huismans Y *et al* 2011 *Science* **331** 61–4
[6] Kuchiev M Y 1987 The two- or three-step model of strong field ionization (Simple Man's model) with purely classical propagation in the electric laser field neglecting the Coulomb potential *JETP Lett.* **45** 404
van Linden van den Heuvell H B and Muller H G 1988 *Multiphoton Processes* ed S J Smith and P L Knight (Cambridge: Cambridge University Press)
Gallagher T 1988 *Phys. Rev. Lett.* **61** 2304
Schafer K J, Yang B, DiMauro L F and Kulander K C 1993 *Phys. Rev. Lett.* **70** 1599
Corkum P B 1993 *Phys. Rev. Lett.* **71** 1994
[7] McPherson A, Gibson G, Jara H, Johann U, Luk T S, McIntyre I A, Boyer K and Rhodes C K 1987 *J. Opt. Soc. Am.* B **4** 595–601
[8] Ferray M, L'Huillier A, Li X, Lompre L, Mainfray G and Manus C 1988 *J. Phys.* B **21** L31
[9] Fittinghoff D N, Bolton P R, Chang B and Kulander K C 1992 *Phys. Rev. Lett.* **69** 2642–5
[10] Walker B, Sheehy B, DiMauro L F, Agostini P, Schafer K J and Kulander K C 1994 *Phys. Rev. Lett.* **73** 1227–30
[11] Feuerstein B *et al* 2001 *Phys. Rev. Lett.* **87** 043003
[12] Brabec T, Ivanov M Y and Corkum P B 1996 *Phys. Rev.* A **54** R2551–4
[13] Comtois D, Zeidler D, Pĕpin H, Kieffer J C, Villeneuve D M and Corkum P B 2005 *J. Phys. B: At. Mol. Opt. Phys.* **38** 1923
[14] Liu C and Hatsagortsyan K Z 2010 *Phys. Rev. Lett.* **105** 113003
[15] Yan T M, Popruzhenko S V, Vrakking M J J and Bauer D 2010 *Phys. Rev. Lett.* **105** 253002
[16] Huang C, Liao Q, Zhou Y and Lu P 2010 *Opt. Express* **18** 14293–300
[17] Liu C and Hatsagortsyan K Z 2011 *J. Phys. B: At. Mol. Opt. Phys.* **44** 095402
[18] Kästner A, Saalmann U and Rost J M 2012 *Phys. Rev. Lett.* **108** 033201
[19] Lemell C, Dimitriou K I, Tong X M, Nagele S, Kartashov D V, Burgdörfer J and Gräfe S 2012 *Phys. Rev.* A **85** 011403
[20] Möller M, Meyer F, Sayler A M, Paulus G G, Kling M F, Schmidt B E, Becker W and Milošević D B 2014 *Phys. Rev.* A **90** 023412
[21] Kelvich S A, Becker W and Goreslavski S P 2016 *Phys. Rev.* A **93** 033411
[22] Blaga C I, Xu J L, DiChiara A D, Sistrunk E, Zhang K K, Agostini P, Miller T A, DiMauro L F and Lin C D 2012 *Nature* **483** 194–7
[23] Bashkansky M, Bucksbaum P H and Schumacher D W 1988 *Phys. Rev. Lett.* **60** 2458–61
[24] Wang X and Eberly J H 2009 *Phys. Rev. Lett.* **103** 103007
[25] Mauger F, Chandre C and Uzer T 2010 *Phys. Rev. Lett.* **105** 083002
[26] Liu C and Hatsagortsyan K Z 2012 *Phys. Rev.* A **85** 023413
[27] Shafir D, Soifer H, Vozzi C, Johnson A S, Hartung A, Dube Z, Villeneuve D M, Corkum P B, Dudovich N and Staudte A 2013 *Phys. Rev. Lett.* **111** 023005
[28] Li M, Liu Y, Liu H, Ning Q, Fu L, Liu J, Deng Y, Wu C, Peng L Y and Gong Q 2014 *Phys. Rev. Lett.* **112** 189901
[29] Perelomov A M and Popov V S 1967 *Zh. Exp. Theor. Fiz.* **52** 514
[30] Ammosov M V, Delone N B and Krainov V P 1986 *Zh. Eksp. Teor. Fiz.* **91** 2008
[31] Daněk J, Hatsagortsyan K Z and Keitel C H 2017 arXiv:1707.06921 [physics.atom-ph]
[32] Pullen M G *et al* 2015 *Nat. Commun.* **6** 7262
[33] Keitel C H and Knight P L 1995 *Phys. Rev.* A **51** 1420–30
[34] Walser M W, Keitel C H, Scrinzi A and Brabec T 2000 *Phys. Rev. Lett.* **85** 5082–5
[35] Milošević D B, Hu S and Becker W 2000 *Phys. Rev.* A **63** 011403(R)
[36] Kylstra N J, Potvliege R M and Joachain C J 2001 *J. Phys.* B **34** L55

[37] Reiss H R 2008 *Phys. Rev. Lett.* **101** 043002
[38] Kohler M C, Pfeifer T, Hatsagortsyan K Z and Keitel C H 2012 Chapter 4—frontiers of atomic high-harmonic generation *Advances in Atomic and Molecular Physics* ed E A Paul Berman and C Lin vol 61 (New York: Academic) pp 159–208
[39] Palaniyappan S, Ghebregziabher I, DiChiara A, MacDonald J and Walker B C 2006 *Phys. Rev.* A **74** 033403
[40] Klaiber M, Hatsagortsyan K Z, Wu J, Luo S S, Grugan P and Walker B C 2017 *Phys. Rev. Lett.* **118** 093001
[41] Hatsagortsyan K Z, Klaiber M, Müller C, Kohler M C and Keitel C H 2008 *J. Opt. Soc. Am.* B **25** B92
[42] Smeenk C, Arissian L, Staudte A, Villeneuve D and Corkum P 2009 *J. Phys.* B **42** 185402
[43] Klaiber M, Yakaboylu E, Bauke H, Hatsagortsyan K Z and Keitel C H 2013 *Phys. Rev. Lett.* **110** 153004
[44] Chelkowski S, Bandrauk A D and Corkum P B 2014 *Phys. Rev. Lett.* **113** 263005
[45] Cricchio D, Fiordilino E and Hatsagortsyan K Z 2015 *Phys. Rev.* A **92** 023408
[46] Chelkowski S, Bandrauk A D and Corkum P B 2015 *Phys. Rev.* A **92** 051401
[47] He P L, Lao D and He F 2017 *Phys. Rev. Lett.* **118** 163203
[48] Dammasch M, Dörr M, Eichmann U, Lenz E and Sandner W 2001 *Phys. Rev.* A **64** 061402
[49] Klaiber M, Hatsagortsyan K Z and Keitel C H 2005 *Phys. Rev.* A **71** 033408
[50] DiChiara A D, Ghebregziabher I, Sauer R, Waesche J, Palaniyappan S, Wen B L and Walker B C 2008 *Phys. Rev. Lett.* **101** 173002
[51] Ekanayake N *et al* 2013 *Phys. Rev. Lett.* **110** 203003
[52] Chirilă C C, Joachain C J, Kylstra N J and Potvliege R M 2004 *Phys. Rev. Lett.* **93** 243603
[53] Mocken G R and Keitel C H 2004 *J. Phys.* B **37** L275
[54] Klaiber M, Hatsagortsyan K Z and Keitel C H 2006 *Phys. Rev.* A **74** 051803
[55] Fischer R, Lein M and Keitel C H 2006 *Phys. Rev. Lett.* **97** 143901
[56] Lin Q, Li S and Becker W 2006 *Opt. Lett.* **31** 2163
[57] Klaiber M, Hatsagortsyan K Z and Keitel C H 2007 *Phys. Rev.* A **75** 063413
[58] Verschl M and Keitel C H 2007 *Europhys. Lett.* **77** 64004
[59] Verschl M 2008 *Laser Phys.* **18** 598–607
[60] Klaiber M, Hatsagortsyan K Z, Müller C and Keitel C H 2008 *Opt. Lett.* **33** 411
[61] Kohler M C, Klaiber M, Hatsagortsyan K Z and Keitel C H 2011 *Europhys. Lett.* **94** 14002
[62] Galloway B R, Popmintchev D, Pisanty E, Hickstein D D, Murnane M M, Kapteyn H C and Popmintchev T 2016 *Opt. Express* **24** 21818
[63] Pisanty E, Hickstein D D, Galloway B R, Durfee C G, Kapteyn H C, Murnane M M and Ivanov M 2016 arXiv:1606.01931
[64] Henrich B, Hatsagortsyan K Z and Keitel C H 2004 *Phys. Rev. Lett.* **93** 013601
[65] Hatsagortsyan K Z, Müller C and Keitel C H 2006 *Europhys. Lett.* **76** 29
[66] Müller C, Hatsagortsyan K Z and Keitel C H 2006 *Phys. Rev.* D **74** 074017
[67] Müller C, Hatsagortsyan K Z and Keitel C H 2008 *Phys. Lett.* B **659** 209
[68] Müller C, Hatsagortsyan K Z and Keitel C H 2008 *Phys. Rev.* A **78** 033408
[69] Kuchiev M Y 2007 *Phys. Rev. Lett.* **99** 130404
[70] Meuren S, Hatsagortsyan K Z, Keitel C H and Di Piazza A 2015 *Phys. Rev. Lett.* **114** 143201
[71] Meuren S, Hatsagortsyan K Z, Keitel C H and Di Piazza A 2015 *Phys. Rev.* D **91** 013009
[72] Førre M, Hansen J P, Kocbach L, Selstø S and Madsen L B 2006 *Phys. Rev. Lett.* **97** 043601
[73] Ludwig A, Maurer J, Mayer B W, Phillips C R, Gallmann L and Keller U 2014 *Phys. Rev. Lett.* **113** 243001
[74] Tao J F, Xia Q Z, Cai J, Fu L B and Liu J 2017 *Phys. Rev.* A **95** 011402
[75] Keil T and Bauer D 2017 *J. Phys. B: At. Mol. Opt. Phys.* **50** 194002
[76] Emmanouilidou A, Meltzer T and Corkum P B 2017 *J. Phys. B: At. Mol. Opt. Phys.* **50** 1225602
[77] Maurer J *et al* 2018 *Phys. Rev.* A **97** 013404
[78] Helm H, Bjerre N, Dyer M J, Huestis D L and Saeed M 1993 *Phys. Rev. Lett.* **70** 3221–4
[79] Eppink A T J B and Parker D H 1997 *Rev. Sci. Instrum.* **68** 3477–84
[80] Parker D H and Eppink A T J B 1997 *J. Chem. Phys.* **107** 2357–62
[81] Ghafur O, Siu W, Johnsson P, Kling M F, Drescher M and Vrakking M J J 2009 *Rev. Sci. Instrum.* **80** 033110
[82] Weger M, Maurer J, Ludwig A, Gallmann L and Keller U 2013 *Opt. Express* **21** 21981–90
[83] Mayer B W, Phillips C R, Gallmann L, Fejer M M and Keller U 2013 *Opt. Lett.* **38** 4265–8
[84] Mayer B W, Phillips C R, Gallmann L and Keller U 2014 *Opt. Express* **22** 20798–808
[85] Pfeiffer A N, Cirelli C, Smolarski M, Dimitrovski D, Abu-samha M, Madsen L B and Keller U 2012 *Nat. Phys.* **8** 76
[86] Nubbemeyer T, Gorling K, Saenz A, Eichmann U and Sandner W 2008 *Phys. Rev. Lett.* **101** 233001
[87] Smeenk C T L, Arissian L, Zhou B, Mysyrowicz A, Villeneuve D M, Staudte A and Corkum P B 2011 *Phys. Rev. Lett.* **106** 193002
[88] Wollenhaupt M, Krug M, Köhler J, Bayer T, Sarpe-Tudoran C and Baumert T 2009 *Appl. Phys.* B **95** 647–51
[89] Dimitrovski D, Maurer J, Stapelfeldt H and Madsen L B 2014 *Phys. Rev. Lett.* **113** 103005
[90] Eckle P, Smolarski M, Schlup F, Biegert J, Staudte A, Schöffler M, Muller H G, Dörner R and Keller U 2008 *Nat. Phys.* **4** 565–70
[91] Eckle P, Pfeiffer A N, Cirelli C, Staudte A, Dörner R, Muller H G, Büttiker M and Keller U 2008 *Science* **322** 1525–9
[92] Landsman A S, Weger M, Maurer J, Boge R, Ludwig A, Heuser S, Cirelli C, Gallmann L and Keller U 2014 *Optica* **1** 343–9
[93] Camus N, Yakaboylu E, Fechner L, Klaiber M, Laux M, Mi Y, Hatsagortsyan K Z, Pfeifer T, Keitel C H and Moshammer R 2017 *Phys. Rev. Lett.* **119** 023201
[94] Delone N B and Krainov V P 1991 *J. Opt. Soc. Am.* B **8** 1207–11